TECTONICS, VOL. 19, NO. 4, PAGES 707-722 AUGUST 2000

Geometry and rate of faulting in the North Baikal Rift, Siberia

Vladimir San'kov,[1] Jacques Déverchère,[2] Yves Gaudemer,[3] Frédérique Houdry,[2] and Andreï Filippov[1]

Abstract. We present a detailed morphotectonic analysis of late Quaternary faulting in the North Baikal Rift (NBR), a region characterized by ranges and basins distributed over more than 800 km along strike in eastern Siberia. Remote sensing techniques (SPOT, METEOR scenes, and aerial photographs) are used to map the active fault network which displays a general en échelon distribution from the northern Lake Baikal to the easternmost basin, with ~30-km-spaced overstepping segments of 10-80 km in length. Most faults have a dominant dip-slip component over their Cenozoic history. The inherited crustal fabric strongly influences the overall geometry of the rifted basins. We use 54 ^{14}C ages of postglacial terraces near the foot scarps of the Muya basin to date offsets measured inside alluvial fans. The last main postglacial event in this area appears to be the early Holocene optimum dated at ~10 ± 2 ka, following the onset of deglaciation at ~13 ka. Using these time constraints, a detailed leveling across two terraces offset by the Taksimo fault (West Muya basin) shows consistent minimum vertical slip rates of 1.6±0.6 mm yr^{-1}. Using 30 other active scarps analyzed in the field, we find a lower bound for horizontal velocity of 3.2±0.5 mm yr^{-1} across the NBR, a rate close to the one found in the southern rift from Global Positioning System measurements. We then compare directions of slip vectors from Holocene field data and slip directions from earthquake fault plane solutions: although local discrepancies appear, the mean directions of lesser horizontal stress (σ_3) inverted from theses values are ~N130°E and ~N155°E, respectively, which are comparable within uncertainties and favor a rifting obliquity of ~30°-40°. Extrapolating our Holocene rates, we estimate basin ages younger than those generally believed (less than 7 Ma) and propose a spatial and temporal evolution of rifted basins consistent with experimental models of oblique rifting. Total amounts of extension and vertical throw (~7 and ~12 km, respectively) across major faults appear rather constant from the central to the northern rift. These results favor a progressive development of asymmetric grabens in a rift zone that widens with times and they indicate a strong rheological control on deformation which seems enhanced by other contributions than the far-field effects of the Indo-Eurasian collision.

[1] Institute of the Earth's Crust, Siberian Branch, Russian Academy of Science, Irkutsk.

[2] Géosciences Azur, Unité Mixte de Recherche 6526 du Centre National de la Recherche Scientifique, Université Pierre et Marie Curie, Villefranche sur Mer, France.

[3] Laboratoire de Tectonique, Unité Mixte de Recherche 7578 du Centre National de la Recherche Scientifique, Institut de Physique du Globe, Paris.

Paper number 2000TC900012.
0278-7407/00/2000TC900012$12.00

1. Introduction

The Baikal Rift, southeastern Siberia, is one of the largest continental rifts in the world. Its topographic expression is outstanding: stretching over 1800 km, it consists of narrow (30-80 km), elongated (100-300 km), and deep basins (up to 7.5 km including sediments), bounded by mountain belts reaching 3000 m in elevation [*Tapponnier and Molnar,* 1979; *Logatchev,* 1993]. This morphology appears mostly rift-related, at least around Lake Baikal itself [*Hutchinson et al.*, 1992; *Van der Beek et al.*, 1996]. The rift system is underlined by a high-level seismicity, especially in its northern part where the seismically deforming area is widening [*Golenetsky,* 1990; *Déverchère et al.*, 1991, 1993]. Both large- and small-magnitude earthquakes indicate a dominant extensional stress field in the central and northern parts of the rift [*Solonenko et al.*, 1993, 1997; *Petit et al.*, 1996], contrasting with active thrusts and strike-slip faults observed in areas located farther south [e.g., *Baljinnyam et al.*, 1993]. While several recent studies have focused on global kinematics and strain models of Asia [e.g., *Avouac and Tapponnier*, 1993; *Holt et al.*, 1995; *Peltzer and Saucier*, 1996; *England and Molnar*, 1997] and on the detailed geometry and relationships of structures limiting the basins [*Solonenko et al.*, 1985], little attention has been paid so far to the significance and rates of deformation at long timescales in this northernmost part of deforming Asia.

As a step toward these objectives, we have performed a morphotectonic analysis of the North Baikal Rift (NBR; Figure 1), which represents only half of the whole rift system. Using satellite images, aerial photographs, and field studies, we have mapped all significant active faults and characterized their geometry. On the field we have measured offsets of morphological features at nine sites in order to determine the slip rate on each fault and its kinematics. We have also used published measurements of cumulative offsets along several faults in the region in order to constrain the regional kinematics. We then discuss our results in the light of two recent studies: one on the stress field and predicted slip directions on faults deduced from fault plane solutions of earthquakes [*Petit et al.*, 1996] and another one on the instantaneous velocity field measured by Global Positioning System (GPS) in the South Baikal Rift [*Calais et al.*, 1998].

2. Active Faults of the North Baikal Rift

2.1. Overall Configuration of Active Fault Segments

In the central part of the NBR, normal faulting is distributed over a region ~250 km wide [*Déverchère et al.*, 1993]. At tips of the NBR, active extension remains confined within single half

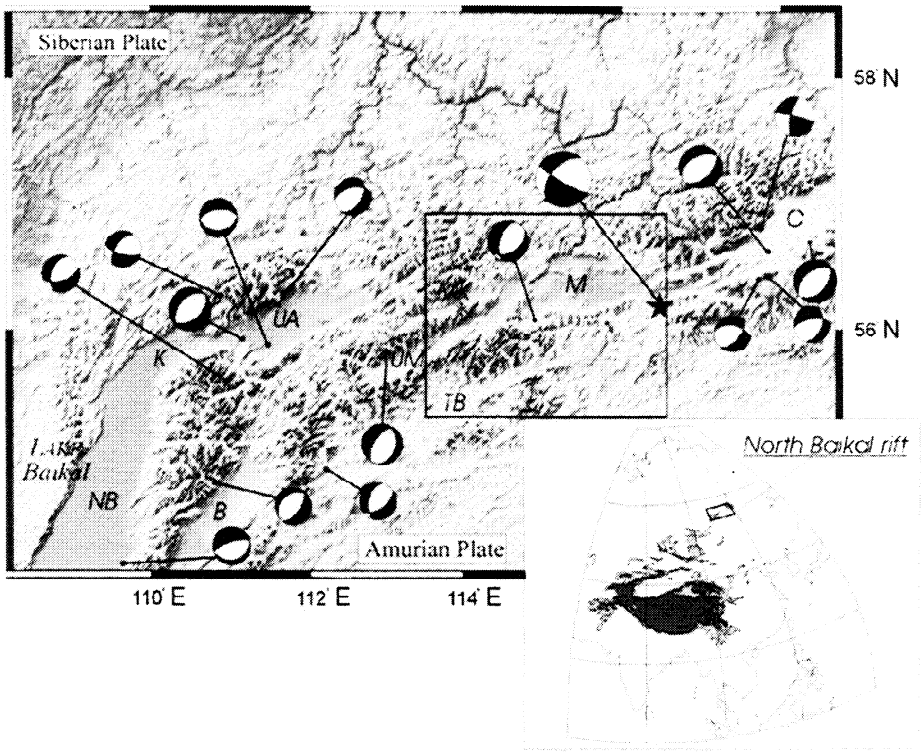

Figure 1. Topog aphy and main focal solutions in the North Baikal Rift (NBR). Inset shows the geographic position of the NBR in the India-Asia collisional system. Focal mechanisms of $M > 5.5$ earthquakes are selected from *Doser* [1991], *Solonenko et al.* [1997], and the Centroid Moment Tensor Solution database of Harvard University. Size of spheres is proportional to magnitude. Square locates the approximate position of the METEOR image (Figure 2). NB, North Baikal Lake; K, Kitchera basin; B, Barguzin basin; UA, Upper Muya basin; MK, Muyakan basin; UM, Upper Muya basin; M, Muya basin; TB, Tsipa-Baunt basin; C, Chara basin. Star is the epicenter of the June 27, 1957, $M = 7.6$ earthquake.

grabens (North Baikal basin and Chara-Tokka basin, 80 and 40 km wide, respectively). Although the overall trend of the NBR is WSW-ENE, it is segmented into smaller, generally asymmetric grabens oriented from N20°E (North Baikal basin) to E-W (Muya basin). On this basis, the NBR may be subdivided into three structurally different parts (Figure 1):

1. West of 111°E, major normal faults dip to the E-SE, bounding half grabens of North Baikal, Kitchera and Barguzin. Faults reach total lengths of 200-350 km but are composed of two or three segments less than 120 km long. The normal faults with the clearest morphology run along the northern Lake Baikal nearly continuously and strike N20°E, nearly parallel to the ancient suture between the Siberian Craton and the Sayan-Baikal mountain belt [*Logatchev and Zorin*, 1992; *Logatchev*, 1993], located 15-50 km west of the lake.

2. Between 111°E and 115°E, in the widest section of the rift, five parallel (main) active faults limit four tilted blocks 30-60 km wide (from Upper Angara (UA) to Tsipa-Baunt (TB) basin, Figure 1). All these faults, except the northern one, the south dipping North Angara fault, dip to the NW. At a detailed scale the normal faults whose maximum lengths reach 80 km consist, in fact, of individual segments with typical lengths of 10-30 km (Figure 2, western part). From the scale of the entire fault down to individual segments, the overall structure is that of a right-stepping, en échelon geometry, widely overlapping, consistent with a left-lateral component of movement in a W-E direction (Figures 1 and 2). Most faults trend around N60°E, which is the main inherited structural direction in this part of the Sayan-Baikal mobile belt [*Zamarayev and Ruzhich,* 1978].

3. East of 115°E, the basins display symmetric (Muya basin) to asymmetric (Chara-Tokka basins) patterns and remain confined in a narrower zone. Fault segments have various strikes (E-W to N-S) and lengths (from 10 to 80 km) and affect the thick and cold Proterozoic crust of the Aldan Craton [*Zamarayev and Ruzhich,* 1978]. It is interesting to note that the bending of rift structures from NE to E-W in the western edge of this region takes place exactly where extensional structures cross the N-S bending of old Proterozoic structures.

2.2. Fault Scarp Morphology

The dip-slip component of faults in the NBR is particularly clear in the morphology on satellite images and on topographic maps (Figures 2 and 3). Mountain fronts are characterized by alignments of steep-faceted spurs, typical of active normal faulting [*Wallace,* 1977]. In this study we evidence for the first time at the scale of the NBR, three generations of scarps with cumulative offsets (Figure 2), which are commonly observed

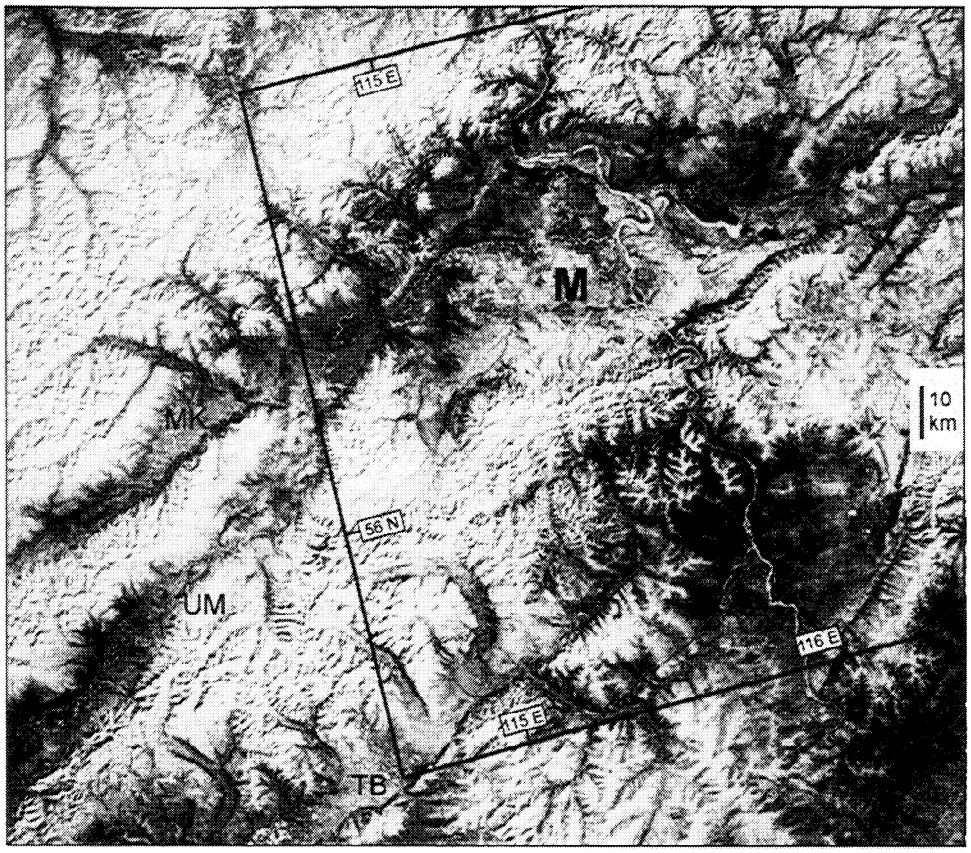

Figure 2. Satellite (METEOR) image (50-m ground resolution) covering the regions of the Muyakan, Upper Muya, Muya (M), and Tsipa-Baunt basins. Note the general step-over pattern of faults, the clear half-graben geometry of the Muyakan, Upper Muya, and Tsipa-Baunt, the diamond shape of Muya, and the very constrasting heights of active scarps (S1 and S2), revealing different ages of fault activities (details in text). See Figure 1 for location. Square locates Figure 3.

along normal faults elsewhere in Asia, for example, in the north China rifts [*Zhang et al.*, 1998]. The highest scarps, which we call S1, 200-800 m high, correspond to offsets accumulated during the last million years at least and are strongly eroded by ice-fields and rivers. The intermediate generation, called S2, shows well-preserved, typical triangular faceted spurs 200-500 m high (Figures 2 and 3). A quite similar morphology for S1 and S2 is found along the master fault of the Northern Baikal basin (with larger throws), where *Hutchinson et al.* [1992] have demonstrated a fault-controlled development of the half graben starting at ~3.5 Ma. Finally, at the base of the mountain fronts, smaller scarps, called S3, offset morphological markers such as coarse-grained fan deltas, alluvial fans, river terraces, or moraines. These scarps are a few meters to a few tens of meters high. They testify for recent movements along the faults. S3 scarps are observed everywhere along the major normal faults of the northern rift, and especially along the northern Baikal basin (e.g., the Kedrovi structure, documented by *Solonenko et al.* [1985] and by *Houdry* [1994]) although both instrumental (last 30 years) and historical (last 300 years) seismicity catalogs do not show any significant event that could be responsible for these scarps. This seismic quiescence probably reflects a time coverage much shorter than the seismic cycle [e.g., *Calais et al.*, 1998]. No striations are generally preserved on the scarps (S3), because they mostly affect detritic deposits. The fresh morphology and the steep scarp slopes often observed (from 25° to 45°) attest for sustained activity and suggest that most of these scarps formed in the past 100 ky [*Wallace*, 1977]. Furthermore, the detritic alluvial fans studied here have a similar size and the same nature in the whole NBR. Finally, it is worth noting that the first stage of fault-related reliefs (S1) is merely absent along the Tsipa-Baunt basin, farther south, and along several fault segments of the Upper Muya and southermost Muya basin (Figure 2). By contrast, the clearest and largest offsets of the S1 generation are observed along the northern Lake Baikal, and the Barguzin, Kitchera, and Upper Angara basins (Figures 1 and 2).

3. Age of Postglacial Terraces

3.1. Glaciations Since 200 kyr B.P. and the Last Deglaciation in Siberia

Previous studies in this part of Siberia [*Bazarov et al.*, 1981; *Endrikhinsky et al.*, 1983; *Trofimov*, 1994; *N. Kulaguina and A. Trofimov*, personal communications, 1992; *Back et al.*, 1999] show that the clear glacial morphology results from the last

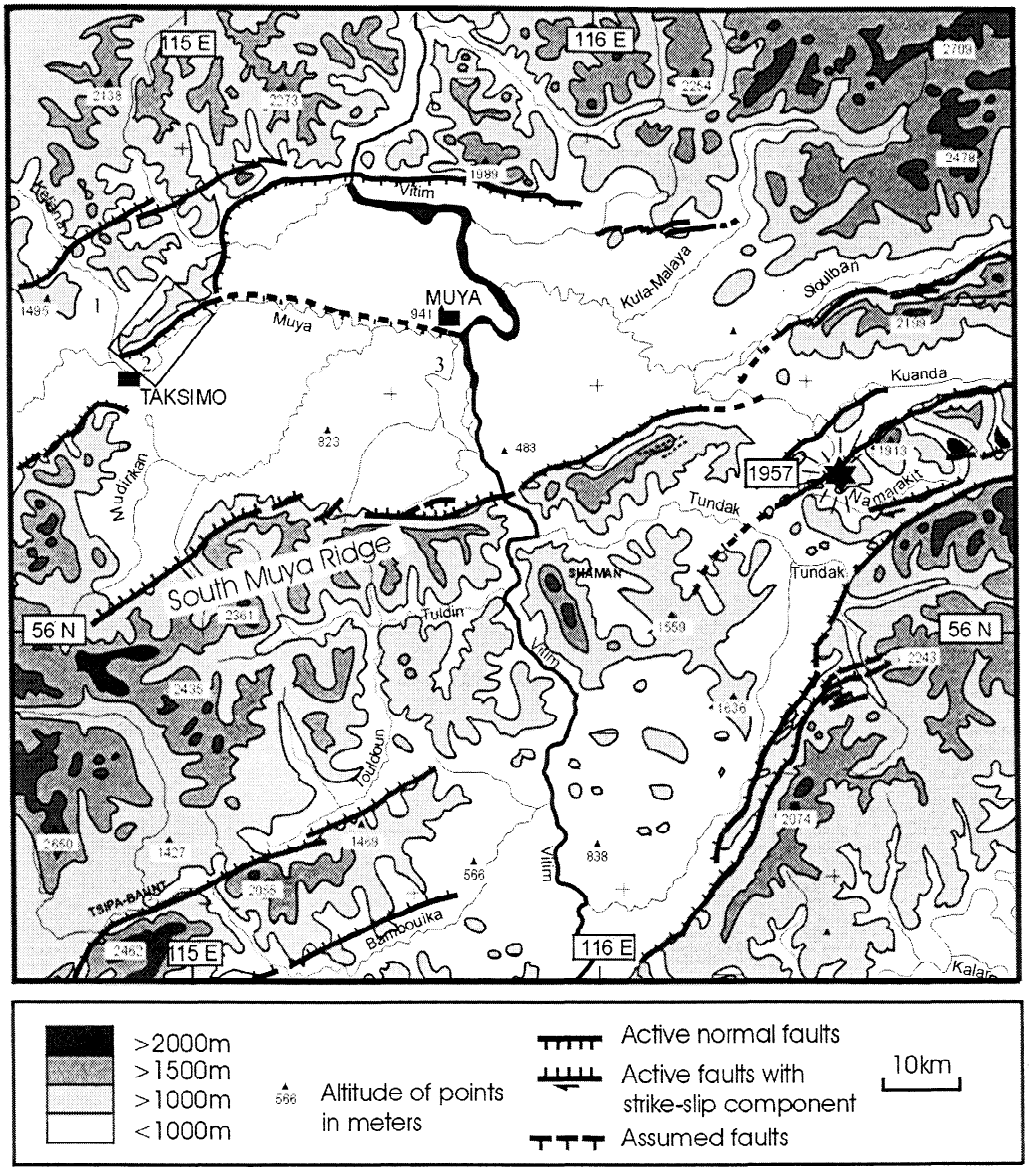

Figure 3. Simplified tectonic sketch of the Muya basin and South Muya range from interpretations of METEOR image (Figure 2) and four SPOT scenes (KJ 266-235, 266-236, 265-235, and 262-235). See Figure 2 for location. Star is the epicenter of the June 27, 1957, M = 7.6 earthquake. Numbers 1, 2, and 3 refer to zones of terrace datings reported in Table 1 along rivers Keliana, Muya, and Vitim, respectively. The dip-slip fault north of Zone 2 is the Taksimo fault scarp (Figure 5). Square locates Figure 5a.

Pleistocene glaciations which correspond to the Riss and Würm cycles. Riss glaciation corresponds to the main glacial southern front with large masses of stagnant ice in basins, while the Würm stage was supposedly of lesser extent, with glaciers confined in valleys within reliefs. Between these two cold phases the interglacial is dated from 130 to 140 kyr B.P.

In the northern Lake Baikal at least three extensive late Pleistocene glaciation pulses have been documented at > 50 ka, 40-35 ka, and 26-13 ka, respectively [*Back and Strecker,* 1998]. The last warming after the Würm glaciations is the most important event to date since it is likely that both the terraces and scarps described here postdate the last glacial maximum. This latter age of 13 ka agrees with at least four other estimates of the onset of deglaciation in Siberia: (1) *Klein* [1971] dates it at ~13 ka from radiocarbon determinations of archeological sites and sedimentological and paleontological data; (2) *Grosswald* [1980] proposed 13.5 ka from major changes in the drainage of large Siberian proglacial lakes; (3) *Colman et al.* [1995] provide an age of 13 ka from pronounced biogenic deposition in Lake Baikal; and (4) *Peck et al.* [1994], by analyzing whole core magnetic susceptibility of sediments from Academician Ridge, central Lake Baikal, show a good correlation of radiocarbon ages between three cores, revealing a last glacial to interglacial transition at ~13 ka. This latter age thus seems to correspond

remarkably well with a clear climatic change in the Baikal region. Furthermore, it coincides with the rapid global warming marking the onset of the present interglacial period, dated between 14 and 11.5 ka [*Bard et al.*, 1991], culminating at the early Holocene optimum dated at 10±2 ka, and ending at 6 ka, as recognized in other parts of Asia [e.g., *Peltzer et al.*, 1988; *Gasse et al.*, 1991; *Gaudemer et al.*, 1995].

3.2. Postglacial Terraces Dated in the Muya Basin

Dating morphological objects offset by faults (alluvial fans, moraines, and terraces) has become a classical tool for constraining slip rates along faults. The most common techniques are the ^{14}C dating of organic matter contained in soils that cover these morphological objects and the use of cosmogenic isotopes, mostly ^{10}Be, to measure the exposure age of quartz-rich pebbles stored at or near the surface of these objects [e.g., *Ritz et al.*, 1995; *Van der Woerd et al.*, 1998]. In the NBR, two or three levels of postglacial terraces are often well preserved along rivers and streams, such as the Muya, Vitim, and Keliana rivers (Figure 3). A recent compilation of more than 400 ^{14}C datings on paleosoil layers in central and south Siberia has shown a mean distribution with a large increase in soil formation at 45-37 ka, and two smaller but clear peaks at 11.3–8.0 ka and 6.0–2.0 ka [*Levi et al.*, 1998]. By comparing these results with those from *Back and Strecker* [1998], it appears that a clear correlation at both global and regional scales exists for a warm period at 9.5 ± 2 ka following the onset of deglaciation at ~13 ka.

In order to get more reliability and accuracy on this timing, we present here a set of 47 new ^{14}C ages from samples collected along the terraces of the Muya, Vitim, and Keliana rivers, in the Muya basin, complementing seven previously published data (Table 1 and Figure 3). Most samples on each terrace are downstream from the faults, but it appears that ages are similar on both sides of the faults. We plot ^{14}C ages against heights of sampled layers within terraces above present-day river levels (Figure 4). Five levels of terraces have been sampled, but the correlation from one river to another is not easy, because some deposits seem linked to transient paleolakes of unknown extent [*Kulchitsky et al.*, 1997]. Although river entrenchment may have been rather different between these three rivers because of different base levels, it appears that the elevation of the sampled layers relative to the river level is roughly proportional to the age determined (Table 1 and Figure 4). We have generally considered ages from layers close to the base of each terrace for dating the onset of terrace formation (Table 2). Among the nine oldest samples (ages more than 23 ka), three are within the outer terrace, but six are found within lower levels: they are considered as reworked material from deposits upstream, as is frequently observed [e.g., *Van der Woerd et al.*, 1998]. Finally, six samples depict very young ages (< 700 years): they probably represent recent flash floods above lower terraces and are discarded (Table 1). Despite these limits, most sample ages are consistent and tend to cluster about values that are clearly distinct from one terrace to the other (Figure 4). For terraces at mean elevations of 30, 20, 15–18, 12, and 6–7 m above rivers, we estimate mean ages of 28±2, 17±2, 10.3±2.0, 6.2±0.5, and 2.5±0.5 kyr B.P., respectively, providing here maximum standard errors (Table 2). Considering the late Pleistocene glaciations documented by *Back and Strecker* [1998] and the previous discussion, we can therefore postulate that the oldest terrace (30 m) consists of

Table 1. List of 54 ^{14}C Datings Made on Samples Collected Along the Inset Terraces of the Muya, Vitim, and Keliana Rivers, in the Muya Basin

Sample Number	Height of Terrace a.r., m	Height of Sampled Layer a.r., m	Age, years	± 1σ, years	Reference
		Keliana River			
1	7	6	120*	30	this study
2	7	6	455*	35	"
3	7	6	500*	55	"
4	7	3.6	1430	40	"
5	7	3.6	1550	65	"
6	7	2.7	2070	50	"
7	7	2.7	2200	55	"
8	7	1.8-2.1	2620	45	"
9	7	1.8-2.1	2730	70	"
10	7	2.7	4065	90	"
		Muya River			
11	12	3.3	7185	355	"
12	6	2	3440	35	1
13	6	1	3500	35	1
14	6	4.7	3280	35	1
15	7	5.5	1960	35	this study
16	7	2	2901	30	"
17	7	2	3010	55	"
18	12	3.5	7195	330	"
19	12	5	4685	80	"
20	12	5	4770	40	"
21	12	5.0	4560	45	"
22	12	5.0	4685	80	"
23	12	4.0	6770	35	"
24	12	4.0	6770	40	"
25	12	3.0	7185	70	"
26	12	3.7	7745	55	"
27	12	3.7	8505	55	"
28	15	14.8	7930	40	"
29	15	11.5	9670	60	"
30	16-18	13.5	10260	220	1
31	16-18	11.4	12920	220	1
32	30	19.5	26760	360	this study
33	30	6.2	27025	320	"
34	30	5.5	27470	320	"
35	30	5.5	27630	385	"
36	30	8.0	28465	420	"
37	30	19.5	29860	260	"
38	30	19.5	34180	1350	"
39	31	7.4	23455	500	"
40	31	11	27515	440	"
		Vitim River			
41	7	2	2300	10	2
42	7	5.6-5.9	220*	50	this study
43	7	5.6-5.9	290*	30	"
44	7	5.1-5.3	2270	35	"
45	7	5.1-5.3	2475	40	"
46	12	6	690*	180	"
47	12	2	8590	130	"
48	12	3	6590	50	"
49	12	4	5370	160	"
50	12	5	3520	150	"
51	16	14	10995	400	2
52	20	16.5	16460	460	this study
53	20	19	16590	610	"
54	20	16.4	17930	680	"

See Figure 3 for location; a.r., above river. References are as follows: 1, *Kulchitsky et al.* [1997]; 2, *Endrikhinsky et al.* [1983].

* Values not selected for computation of mean ages in Table 2 (see text for details).

Table 2. Average Values, Weighted Mean and Median Mean, of Ages Sampled in the Terraces of the Three Rivers Studied in the Muya Basin, After Selection of Consistent Data from Table 1

Height of Terrace	River	Number of Sampled Layers Used	Age, years	
			Average Mean Value (Weighted)	Average Mean Value (Median)
~30 m	Muya	9	27,783 ± 125	28,151 ± 484
~20 m	Vitim	3	16,828 ± 323	16,993 ± 584
~15-18 m	Muya, Vitim	5	8118 ± 32	10,355 ± 188
~12 m	Muya, Vitim	14	6264 ± 15	6210 ± 95
~6-7 m	Muya, Vitim, Keliana	16	2464 ± 8	2613 ± 45

See text for details.

deposits from the deglaciations between cold periods of 40–35 ka and 26–13 ka, while the 17±2 ka old deposits in the Vitim area, rarely sampled and poorly preserved, could be linked to proglacial lakes [*Grosswald*, 1980]. Well-preserved terraces 15–18 m high thus date the early postglacial warming at ~10 ka.

4. Holocene throw rates and displacement vectors

4.1. The Taksimo Fault Scarp and Shifted Terraces

The very dense vegetation cover in Siberia has prevented us from carrying out an exhaustive survey including systematic offset measurements. Fortunately, at one site near Taksimo (Figure 3), the bedrock is outcropping around a major, linear fault, located at the westernmost tip of the Muya basin fault (at ~56.3°N and 114.9°E, Figures 2 and 3). Since accurate datings are numerous around this place, it is hence a good opportunity to carry out for the first time a dense and accurate geomorphic leveling in the NBR. The relief along the Taksimo fault does not exceed 1500 m, and the linearity of crests and slopes, yet weakly eroded, attests for a first generation of preserved facets (S1) ~500–700 m high. Furthermore, the well-expressed alignment of triangular faceted spurs (S2) and the tectonic control of the Muya river along the fault evidence a very young, active normal fault (Figure 5). At the base of the triangular facets (S2) 200 to 300 m high, a network of subparallel scarps (S3), oriented N50°E and 15 km long at least, clearly disrupts sediments accumulated in the piedmont. Near two landslides visible on facets S2 (perhaps triggered by earthquakes), we have studied a large detritic fan where three levels of terraces are recognized (Figure 6). The fault appears to be discontinuous (Figure 5), showing short, parallel fault segments (sometimes disposed en échelon) and tension cracks striking along the slope break. The three terraces have locally preserved a good record of vertical cumulative offsets. No

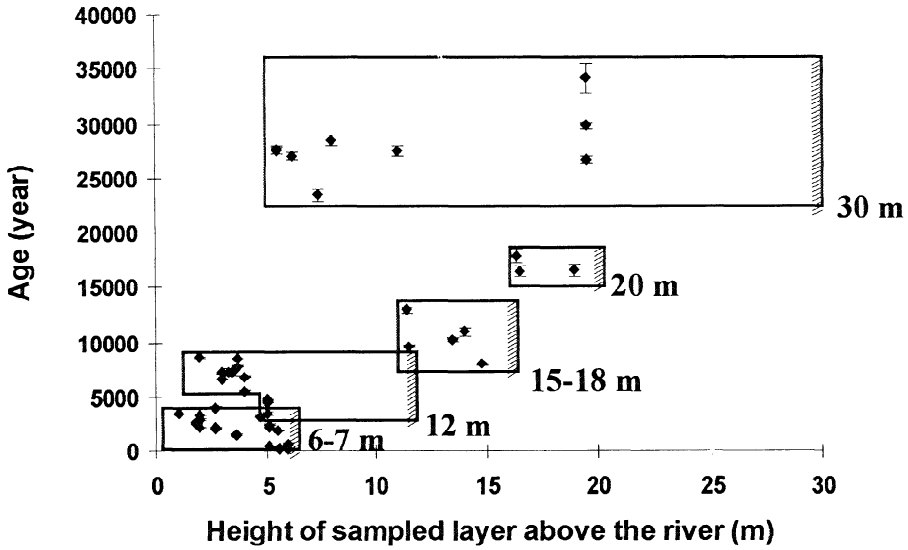

Figure 4. Plot of 54 ^{14}C sample ages as a function of increasing height of samples relative to the present river height, for each terrace of the Muya, Vitim, and Keliana rivers, in the Muya basin (see Figure 3 for location and Table 1 for standard errors and positions relative to rivers). Alluvial surfaces are at 6-7, 12, 15-18, 20, and 30 m, respectively. Note the pattern of clustering around mean values, the general linear increase of ages versus alluvial surface heights, and the short wavelength decrease of ages versus heights inside the younger terraces (7, 12, and 15-18 m, respectively). Boxes gather the samples assumed to belong to each terrace (see text).

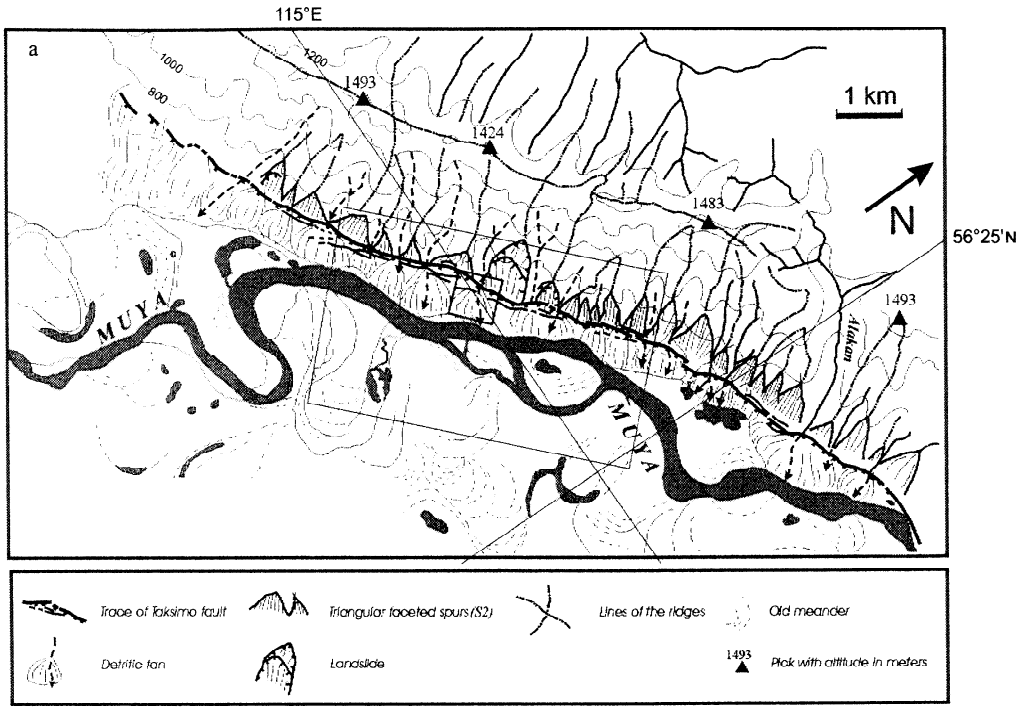

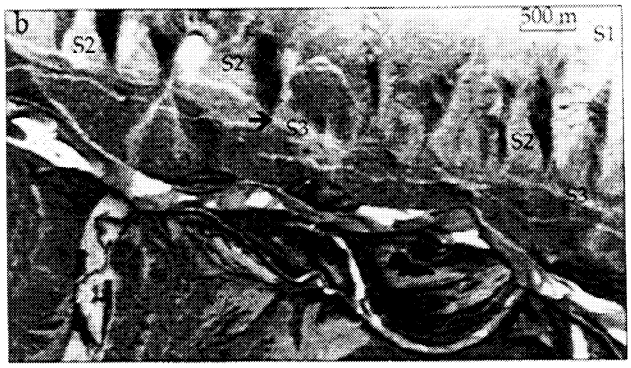

Figure 5. (a) Morphotectonic interpretation of the Taksimo fault after interpretation of SPOT image KJ 262-235 (October 12, 1991). See Figure 3 for location. S1 (500-700 m high, from the crests to the top of triangular faceted spurs) and S2 (200-300 m high, triangular faceted spurs) depict the two oldest generations of cumulative scarps (see text). Square shows location of Figure 6. (b) Detail of the SPOT scene indicated by large box in Figure 5a. Black arrow depicts the place of field measurements on terraces (S3 scarps).

horizontal displacement is observed on this fault. The stream is a tributary of the Muya river, which is at less than 1 km to the south (Figure 5). The scarp cutting the successive stream deposits shows both smaller heights and steeper morphologies where it offsets the younger terrace, near the present stream bed. Individual normal offsets range from 2 to 10 m. The smallest offset observed (2 m, A in Figure 6) could represent the coseismic displacement released by a single earthquake, although we have no way to check it. Profiles T1 and T2 (Figures 6c and 6d) depict total vertical offsets from the mean surface of the fan of 9.2±1.6 and 16.4±1.7 m, respectively.

Taking into account the position of the stream with respect to the Muya river, we may use the interpretations of the postglacial terraces dated in the Muya basin to infer minimum velocities. The first terrace (Tc), poorly eroded by the stream, is younger than or has the same age as the terrace 7 m high of Muya river, for which the age determined by ^{14}C dating is 2.5±0.5 ka. Terrace (Tb), only about 7 m above, thus corresponds at the most to the terrace 12 m high of Muya river, dated at 6.2±0.5 ka. Finally, the outer terrace (Ta) ~14 m above the present stream bed has to be correlated with the 15–18 m high terrace of Muya, dated at 10.3±2.0 ka (Table 2 and Figure 4). It is thus reasonable to assume that the last Holocene warming is responsible for the formation of the outer terraces described here and probably of the detritic fan too. Assuming that the two oldest terraces (Ta and Tb, Figure 6b) on profiles T2 and T1 (Figures 6c and 6d) are 10.3±2.0 and 6.2±0.5 ka, we find average vertical slip rates during the Holocene of 1.6±0.6 and 1.5±0.4 mm yr^{-1}, respec-

Table 3. List of 31 Sites Selected at the Foot of Active Faults in the North Baikal Rift for Which a Holocene or Younger Displacement is Inferred

Fault System and Basin	Individual Fault	Latitude N, deg	Longitude E, deg	Length, km	Strike, deg N	Vertical Offset, m	Horizontal Offset, m	Reference
North Baikal	Solontsovaya	54.1	108.2	30	45	10-12	0?	1, 2
North Baikal	Kedrovi	54.4	108.5	10-15	25	10	0	1, 2
North Baikal	Khibelenskaya	54.8	108.8	22	45	8	0	1, 2
Kitchera	Kitcherskaya	56.0	110.1	26	65	4-6	0	2
Kitchera	Gaenda *	55.9	109.8	30	75	5	30? L	this study
Kitchera	Dzelinda	56.1	110.6	20	60	6	0	2
Barguzin	Barguzin 1,2,3	54.2	110.5	30,15, 20	30, 45, 50	11, 13, 15	3 L, 0, 0	2
Upper Angara	North Angara	56.4	111.5	15-80	60	>10	0?	this study
Upper Angara	Yanchukan	56.2	112.9	6	60	15	0	this study
Upper Angara	Gonkuli *	56.1	112.5	5	70	>10	30? L	this study
Kovokta	Kovokta	56.2	113.1	30	60	8	0	1
Muyakan	Arkum *	56.2	113.9	15	55	2	0	this study
Muyakan	Oulga	56.2	113.7	25	60	7	5 L	this study
Upper Muya	Upper Muya	55.8	113.5	20-90	60	6	6 L	2
Tsipa-Baunt	Baunt 1,2	55.5	114.2	20, 15	60, 65	15, 12	0	2
Muya	North Muya	56.6	115.4	9	95	19	0	1, this study
Muya	Moudirikan	56.3	115.6	20	90	20	0	this study
Muya	Taksimo	56.1	114.8	15	50	16	0	this study
Muya	Muisk *	56.0	116.8	35	90	3	1 L	2
Chara	Baronka	56.4	117.0	8	80	9	12 L	2
Chara	Sakoukansk 1,2	56.8	117.8	5, 3	65, 20	5, 4	0, 5 L	2
Chara	Dovatchan 1,2*	56.4	117.4	12, 1	70, 80	7, 2	11 L, 0	2
Chara	Kemen	56.7	118.7	4	65	12	0	2
Chara	China-Medved	56.5	118.9	43, 4	80, 60	9, 5	0	2
Chara	Ebgakhlir	57.3	119.3	7	50	4	0	2

Offsets and lengths of faults are given for individual segments, or sometimes as mean values for several measurements on a continuous fault system. Horizontal offsets are labeled L for left-lateral components. Question marks mean doubtful measurements on horizontal components (river offsets). First column refers to major faults and basins shown in Figure 1. References are as follows: 1, *Solonenko* [1977]; 2, *Solonenko et al.* [1985].

* Sites not used for mean vector computations because of doubtful horizontal offsets or scarps much younger than other ones.

tively, on the Taksimo scarp. This could indicate recurrence times of ~1000–2000 years for earthquakes producing 2 m of average vertical slip.

4.2. Holocene Vectors (Rates and Azimuths) on Major Faults

4.2.1. Criteria for data selection on individual faults. Combining our field observations at nine sites with those described in previous Russian studies [*Solonenko*, 1977; *Solonenko et al.*, 1985], we try to estimate Holocene displacement vectors (*Vm*) along several normal fault scarps (S3 type) in the NBR. We use horizontal and vertical offsets observed on 31 individual faults (Table 3) belonging to 14 main fault systems (Table 4). Criteria of selection of sites are the consistency of throw amounts at each site and from one close site to another and the nature and extent of the deposits offset by the faults. Most shifted deposits are thick alluvial fans or terraces similar to the ones described at the Taksimo site and are therefore assumed to be of Holocene age (10 ± 2 ka) or younger. Along the Kitchera and Upper Angara faults, we have observed two important left-lateral offsets (30 m) of rivers orthogonal to faults (Table 3), which we decided not to take into account in our slip rate estimates. Indeed, it appears that (1) these apparent offsets are probably cumulative displacements older than Holocene, and (2) several mechanisms make the use of apparent river offsets along strike-slip faults a difficult exercise for deriving slip rates [e.g., *Gaudemer et al.*, 1989]. Nevertheless, these observations, together with other additional evidence collected along faults striking in the main structural direction N60°-70°E (gouges, cracks, gullies, systematic left-lateral en échelon geometry at all scales, left-lateral components nearly always detected, etc.) are worth noting and indicate that our measurements may slightly underestimate the actual left-lateral motion on major faults and hence the velocities computed here.

4.2.2. Computing strain rates and azimuths of displacement vectors. We then associate individual site observations with the 14 main faults for which we estimate mean vertical rates (Table 4, column 9). In order to give bounds to horizontal rates and azimuths of Holocene slip vectors (Table 4, columns 2 and 3), we have to use mean values of strike (*S*) and plunge (*P*) of faults. Strikes *S* are obtained from detailed mapping on satellite images and field studies. Plunges *P* are deduced from field observations, mean dips of nodal planes from focal solutions of the area [*Petit et al.*, 1996], depth distribution of earthquakes [*Déverchère et al.*, 1993], or seismic cross sections [*Hutchinson et al.*, 1992]. For the 14 main faults of the NBR investigated here, *P* values appear to vary little around 50°-60°: we choose a mean fault dip of 60° in order to remain within lower bound estimates of horizontal velocities. Since some of the 14 main faults are poorly sampled (Table 3), we group the 31 sites into height main faulted areas (Table 4, column 1) in order to invert the horizontal projection of displacement vectors (*Vm*).

Table 4. Mean Horizontal (*H*) Velocity Vectors Inverted From Holocene Fault Scarps and Long-Term Vertical (*V*) Throws on Each Major Fault of the North Baikal Rift

Main Faulted Areas	Holocene *H* Rate, mm yr^{-1}	Vector Strike, deg N	Main Fault	Mean Basin Altitude, m	Apparent *V* Throw, m	Sediment + Water Thickness, m	Total Throw, m	Holocene *V* Rate, mm yr^{-1}	Long-Term Age, Ma
North Baikal - Kitchera	0.67 ± 0.15	093 ± 13	Central Segment	-400	1700	900 + 3500	6100	1.0 ± 0.2	6.1
	-	-	Northern Segment	-300	900	800 + 4000	5700	1.0 ± 0.2	5.7
	-	-	Kitchera	500	1300	2000	3300	0.5 ± 0.2	6.6
Upper Angara (N)	0.55 ± 0.12	125 ± 15	North Angara	500	2100	2000	4100	1.0 ± 0.3	4.1
Upper Angara (S)	0.75 ± 0.13	144 ± 18	South Angara	600	1500	1000	2500	1.5 ± 0.2	1.6
Barguzin	0.80 ± 0.09	115 ± 12	West Barguzin	500	2400	2500	4900	1.0 ± 0.2	6.1
Muyakan - Upper Muya	0.73 ± 0.17	091 ± 8	Kovokta	1400	600	200	800	0.8 ± 0.1	1.0
	-	-	Muyakan	800	1300	500	1800	0.7 ± 0.1	2.5
	-	-	Upper Muya	1000	1600	500	2100	0.7 ± 0.1	3.0
Muya (N) - Muya (S)	1.31 ± 0.18	159 ± 14	Taksimo	600	900	2200	3100	1.6 ± 0.6	1.9
	-	-	North Muya	500	1700	1000	2700	1.9 ± 0.2	1.4
	-	-	South Muya	500	1800	500	2300	2.1 ± 0.2	1.1
Tsipa-Baunt	0.68 ± 0.25	152 ± 18	South Tsipa-Baunt	1100	900	500	1400	1.3 ± 0.2	1.0
Chara	1.05 ± 0.11	096 ± 4	West Chara	800	1700	1500	3200	1.0 ± 0.1	3.2

Long-term ages (column 10) are obtained by extrapolating the velocities deduced from Holocene vertical offsets on scarps S3 (column 9). Sediments thicknesses in basins are from *Logatchev and Zorin* [1992]. Apparent *V* throws (S2 + S3) are estimated by assuming that mountains range building along the faults is entirely rift related, that is, preexisting reliefs are negligible [*Van der Beek et al.*, 1996; *Van der Beek*, 1997]. Mean basin altitudes are given above sea level. Faults are located in Figure 7. See Table 3 for Holocene fault scarps.

Within each area, we compute values of χ^2, i.e., the root mean square residuals between observed and theoretical offsets, weighted by the squares of standard deviations on L and α, where L and α are the horizontal length and azimuth of vector *Vm*, respectively [*Houdry*, 1994]. Theoretical offsets (vertical and horizontal) are offsets computed for a given fault strike and dip when a finite displacement is applied on this fault. To make the inversion, we make the implicit assumption that faults played contemporaneously. The lowest χ^2 determines the best values of L and α, with error bars given by the domain lower than (χ^2 + 1).

4.2.3. Results and comparison with predicted slip vectors from focal mechanisms. Several striking features appear: First, vertical rates are rather comparable from one fault to another and vary around 1±0.5 mm yr^{-1}, except on the faults of the Muya basin where the vertical rate is about 2 times higher (Table 4, column 9). Second, most faults have a systematic left-lateral component of motion (Table 3 and Figure 7). High rates along Muya basin may come from the fact that the rift system is much more localized there compared to the area between 111°E and 115°E (Figure 7). Azimuths of displacement vectors (horizontal projections, Table 4, column 3) are scattered around a value of N130°E, with angular differences of up to 68° (inset A in Figure 7). From west to east, we observe an apparent alternation of W-E to NW-SE pointing arrows, which go from W-E to SE from Lake Baikal to Upper Angara basin, then again to W-E in Muyakan-Upper Muya-Tsipa Baunt, again to SE in Muya, and finally to W-E in the Chara region. This suggests rotations or possible decoupling effects between different blocks from west to east. A similar style of deformation has been described from the inversion of focal solutions of earthquakes in the same area [*Petit et al.*, 1996]: in this procedure, synthetic ("predicted") slip vectors are obtained by applying stress tensors inverted from focal mechanisms on the main faults (thin solid arrows in Figure 7). Nevertheless, several predicted slip vectors deduced from this latter approach point more to the south than Holocene arrows do: Angular discrepancies are 90° (Kitchera), 58°-74° (Muyakan), 48°-69° (Upper Muya), and 35° (Chara), whereas a good fit is observed in other regions (Figure 7). Three main explanations may be invoked: (1) The strain field may change on a short timescale (less than 10 kyr), possibly in relation to postseismic relaxation after large earthquakes or because of quick stress changes; (2) our time and space sampling of fault plane solutions and fault scarps is not dense enough, which results in sometimes inappropriate strain strike or stress strike predictions on large faults; and (3) seismological and field data discussed here represent only part of the total seismic strain. Taking into account the occurrence of the M = 7.6, June 27, 1957, event, SE of the Muya basin, which reveals a large component of left-lateral strike-slip motion along a WNW-ESE plane [*Doser*, 1991; *Solonenko et al.*, 1997] (Figure 1), we may favor hypothesis 2. Indeed, this event depicts a T axis direction of ~N175°±10°E at the edge of the Muya basin (according to the preferred fault plane solution [*Petit et al.*, 1996]), where both kinds of vectors (from microseismicity and Holocene scarps) show very similar trends (~N170°±10°E, Figure 7). Furthermore, both approaches evidence fast spatial changes of stress directions at short wavelengths (100 km), a fact that favors hypothesis 2. Hence we assume that a more complete description of Holocene fault scarps and a longer time observation of earthquakes could allow us to better identify the limits of deforming blocks in the NBR and

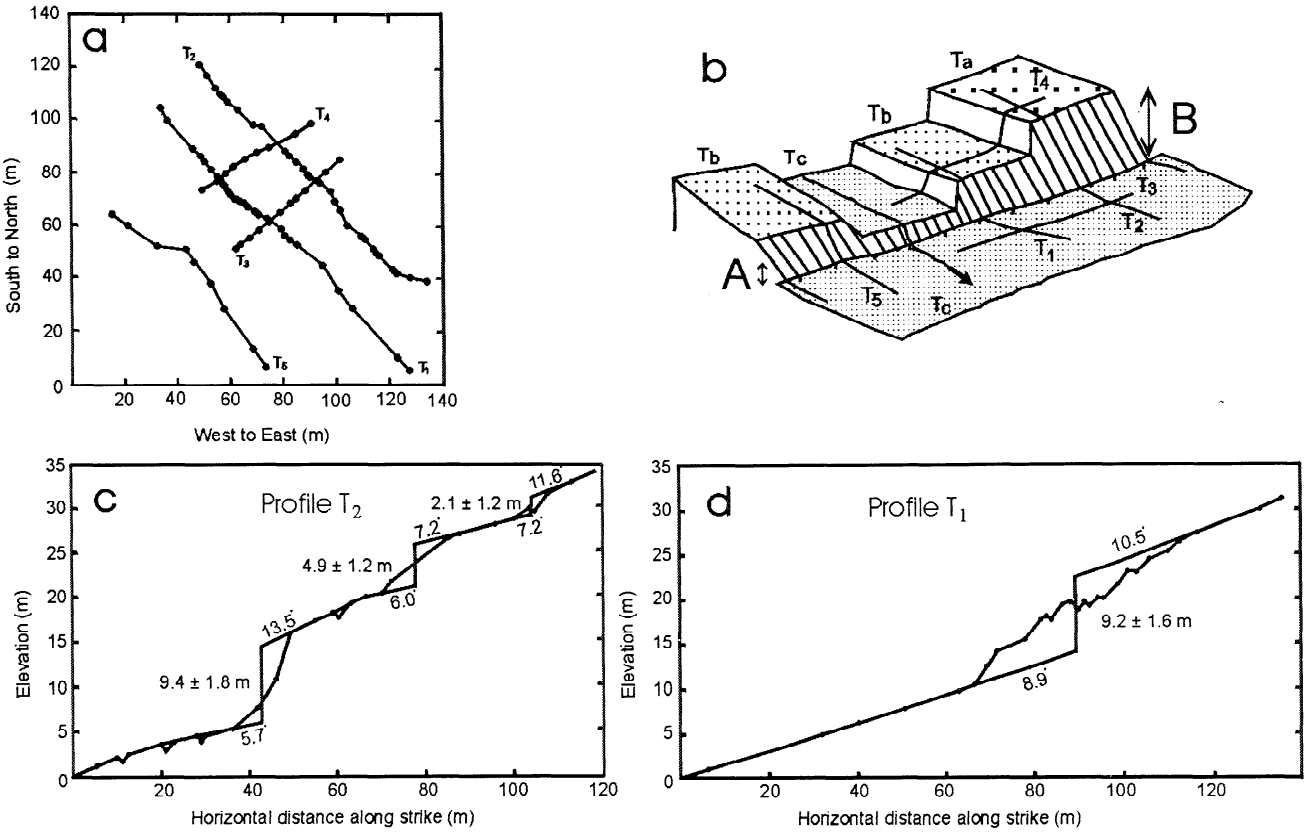

Figure 6. Vertical offsets of terraces and theodolite profiles leveled across the Taksimo fault. (a) Map view of profiles leveled, with measured points as dots. b) Perspective view from south. A (~2 m) and B (~16 m) double arrows show minimum (probably related to one seismic rupture) and maximum cumulative throws, respectively. Ta, Tb, and Tc are outer (or upper), intermediate, and inner terraces, respectively. (c, d) Theodolite profiles T2 and T1 across the outer (Ta) and intermediate (Tb) terraces, respectively. Vertical exaggeration is 2. Values of elevation and distances are in meters, and slopes are in degrees. Downstream, terraces are covered by recent deposits (Tc) from the fan.

thus could explain the apparent discrepancies between these two data sets in our study area.

5. Approximate Direction, Rate and Amount of Extension Across Basins

From the new and systematic survey presented here at the scale of the whole NBR, we may now hypothesize the main strain and stress directions and Holocene rate from one side of the rift to the other, compare them to other strain, stress, and velocity measurements in the Baikal Rift, and tentatively extrapolate the rate found to Plio-Quaternary and Miocene times in order to test the consistency of our results with other geological observations in the study region.

5.1. Mean Horizontal Velocity and Comparison With GPS Results in the Southern Baikal Rift

We may now estimate Holocene lower velocity bounds in the central part of the NBR: Displacements measured on each main fault can be summed on the basis of our inferred Holocene vectors (rates and azimuths) assumed on major faults (Table 4 and Figure 7). By testing different cross sections striking NW-SE, we find mean horizontal velocities varying between 2.7 and 3.7 mm yr^{-1}, in directions ranging from N122°E to N157°E. This provides a mean horizontal velocity vector of 3.2±0.5 mm yr^{-1} trending N140°±20°E. This average velocity is compatible with the instantaneous velocity of 4.5±1.2 mm yr^{-1} deduced by *Calais et al.* [1998] from three years of GPS measurements in the South Baikal Rift, with a mean direction of extension of N110°±30°E. Keep in mind that we have computed a lower bound for Holocene displacements; this result suggests a rather constant space and time displacement field across the Baikal Rift, at least over the last 10 kyr, thus strengthening our previous conclusions.

5.2. Least Horizontal Stress Directions From Scarps and Focal Mechanisms

An average stress direction may also be deduced from our field measurements on Holocene scarps: As for microtectonic data, we apply the right-dihedra method [*Angelier and Mechler,* 1977] to the field offsets (Table 3), converted into slickensides, and their associated fault planes. We do not attempt here to compute a stress tensor, because of a limited fault strike distribution and the lack of accuracy on fault dips. Among the 31 sites, we have discarded 5 of them because of questionable

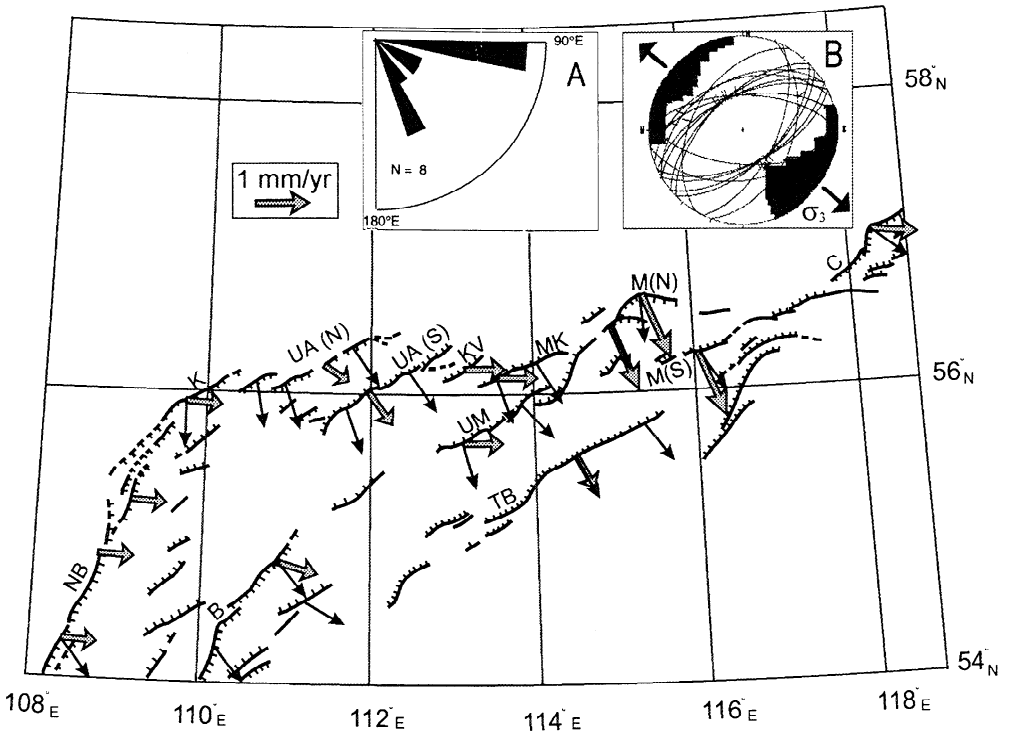

Figure 7. Active faults of the NBR deduced from SPOT, METEOR images, and field analyses, and schematic representation of the strain indicators. Large shaded arrows are Holocene horizontal velocity vectors (azimuths and moduli in mm yr^{-1} taken from Table 4, columns 3 and 2) inferred from field studies applied to the 14 main faults. Solid arrows depict horizontal slip vectors (only strikes) inferred by applying stress tensors deduced from local inversions of focal mechanisms of earthquakes on the main faults [*Petit et al.*, 1996]. Inset A is a rose diagram of the Holocene displacement vector strikes (Table 4, column 3). Inset B shows the 26 striated fault planes and associated slickensides selected from Table 3 on a stereonet, with dips of planes of 60° (dip slip) or 45° (oblique slip); solid areas result from superimposition of the tensional right dihedra of the 26 data after various tests on fault dips: these areas constrain the possible location of the lesser horizontal stress (σ_3), and diverging solid arrows give the average σ_3 direction (N130°E). Small inset gives the scale for Holocene horizontal velocity vectors. Letters refer to Figure 1. S and N are south and north, respectively, and KV is the Kovokta fault.

horizontal offsets at 2 sites (see section 4.2.1) or small offsets which are obviously younger than Holocene at 3 other sites (asteriks in Table 3). We run several tests with dips of faults ranging from 45° to 60°, since this parameter is not easy to measure on S3 scarps. We find a mean strike of the minimum stress axis (σ_3) of N130°±45°E (inset B in Figure 7). Although this value is poorly constrained, it reveals first a mechanical compatibility between the strain indicators on the field. Furthermore, this average azimuth is close to the mean horizontal velocity vector found above. This value is also worth comparing to the average direction of the seven σ_3 stress axes determined by *Petit et al.* [1996] from focal mechanisms (from Kitchera to Chara), which is N154°±10°E (without any weighting in this case), a value indicating mostly dip-slip faulting on main faults. Such angular differences between stress and motion directions are commonly observed in regions of block rotations [e.g., *Manighetti et al.*, 1997]. Given the uncertainties computed, we find no evidence for a strong incompatibility between stress indicators deduced either from earthquakes or from Holocene scarps.

5.3. Possible Age of Basins at Constant Extension Rate and Comparison With Other Estimates

We now extrapolate the vertical Holocene rates found on the 14 main faults to deduce a possible age for basins of the NBR (Table 4). Under the strong assumptions that (1) all reliefs directly above master faults are rift related [*Van der Beek et al.*, 1996; *Van der Beek*, 1997] and thus considered as S3-S2-S1 generations and (2) the velocity field remains stable since at least the "fast-rifting stage", i.e., since the beginning of important modifications of the basin architecture, near 5.3 - 3.5 Ma [*Logatchev and Zorin*, 1987; *Hutchinson et al.*, 1992; *Delvaux et al.*, 1997], we estimate the total throws of the master faults by adding apparent (topographic) throws and water and sediment thicknesses taken from *Logatchev and Zorin* [1992]. Ages obtained (Table 4, column 10) suggest that the basin systems of northern Lake Baikal, Kitchera, and Barguzin have formed more or less simultaneously, followed ~2 Myr later by basins of Upper Angara (as half-graben first), Chara, Upper Muya, and Muyakan, successively. At last, ~1 Myr later, the basins of Muya and Tsipa-

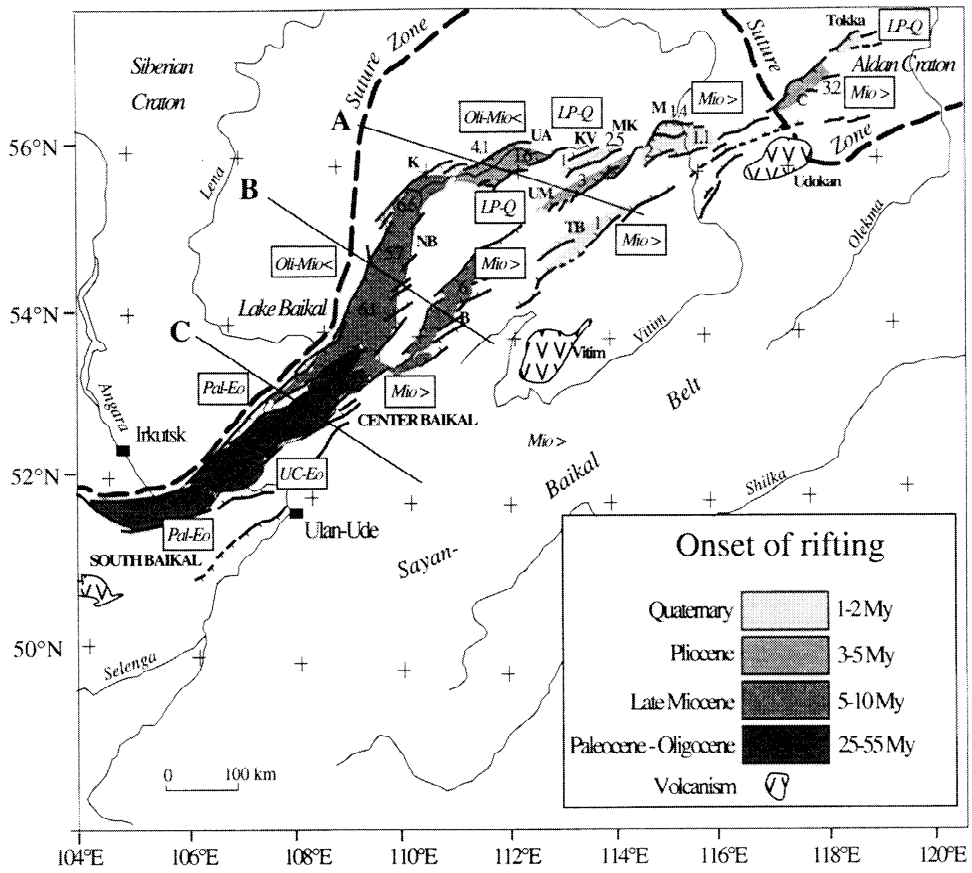

Figure 8. Map of the main basins and faults of the central and North Baikal Rift, with onset of rifting estimated considering constant velocity rates deduced from this study. Numbers near faults are long-term ages of basins obtained by extrapolating our velocity rates on faults (Table 4, column 10). Small inset gives basin ages estimated after *Logatchev and Zorin* [1992] and *Logatchev* [1993], for comparison. Dashed thick lines delineate the Paleozoic suture zone between the old cratons (Siberia and Aldan) and the Sayan-Baikal folded belt. A, B, and C lines are positions of cross sections shown in Figure 9. Letters refer to basin names (same abbreviations as in Figures 1 and 7). UC, Upper Cretaceous; Pal, Paleocene; Eo, Eocene; Oli, Oligocene; Mio, Miocene (<: lower, >: upper); LP-Q, Late Pliocene-Quaternary.

Baunt started, together with the southern side of Upper Angara and small internal depressions like Kovokta (Figure 8). Age values inferred here are generally younger than those postulated by Logatchev and Zorin and *Logatchev* [1993] by about 1-4 Ma, and depict a different chronology (Figure 8). Conversely, the age that we postulate for the northern lake (6.6 Ma) is older than the one inferred by *Hutchinson et al.* [1992], who date the beginning of thick deposition ("middle-rift complex") at 3.4 Ma. These discrepancies in absolute ages may arise from large uncertainties in the methods of dating, and also from the two strong assumptions made here and recalled above. For instance, slip rates may have increased in the last 3 million years, as suggested by indications of recent uplift and subsidence around Lake Baikal [*Mats*, 1993; *Agar and Klitgord*, 1995; *Artyushkov et al.*, 1990]. Nevertheless, relative changes in basin formation and evolution are clear whatever the way of dating them and in spite of these discrepancies (Figure 8). Therefore this spatial rift evolution differs from a simple propagation model of rifting as observed in Africa, for instance [see, e.g., *Manighetti et al.*, 1997].

5.4. Finite Extension in the Central and Northern Baikal Rift

Finally, we estimate the amount of extension and cumulative vertical throws along three transects of the Baikal Rift striking NW-SE, from the central Lake Baikal to the Tsipa-Baunt basins (Figure 9). We have used the published sediment thicknesses [*Logatchev and Zorin*, 1992, and references therein], topographic cross sections, our identification of activity of faults on both sides of half grabens and symmetric basins, and an assumed mean fault dip of 60°. We find rather constant amounts of extension and vertical throws of 7.0±0.5 and 12±1 km, respectively, for the three transects. This amount is less than the crude estimates of total crustal extension by *Zorin and Cordell* [1991], who found 19 and 9 km in the Central and North Baikal Rift, respectively. This discrepancy may arise from our determinations of minimum velocities and our choice of steep fault dips, but also from the inaccuracy of the determination from Zorin and Cordell based on assumptions of mass and volume balance from gravity data. Whatever the case, it is interesting to note that the North Baikal

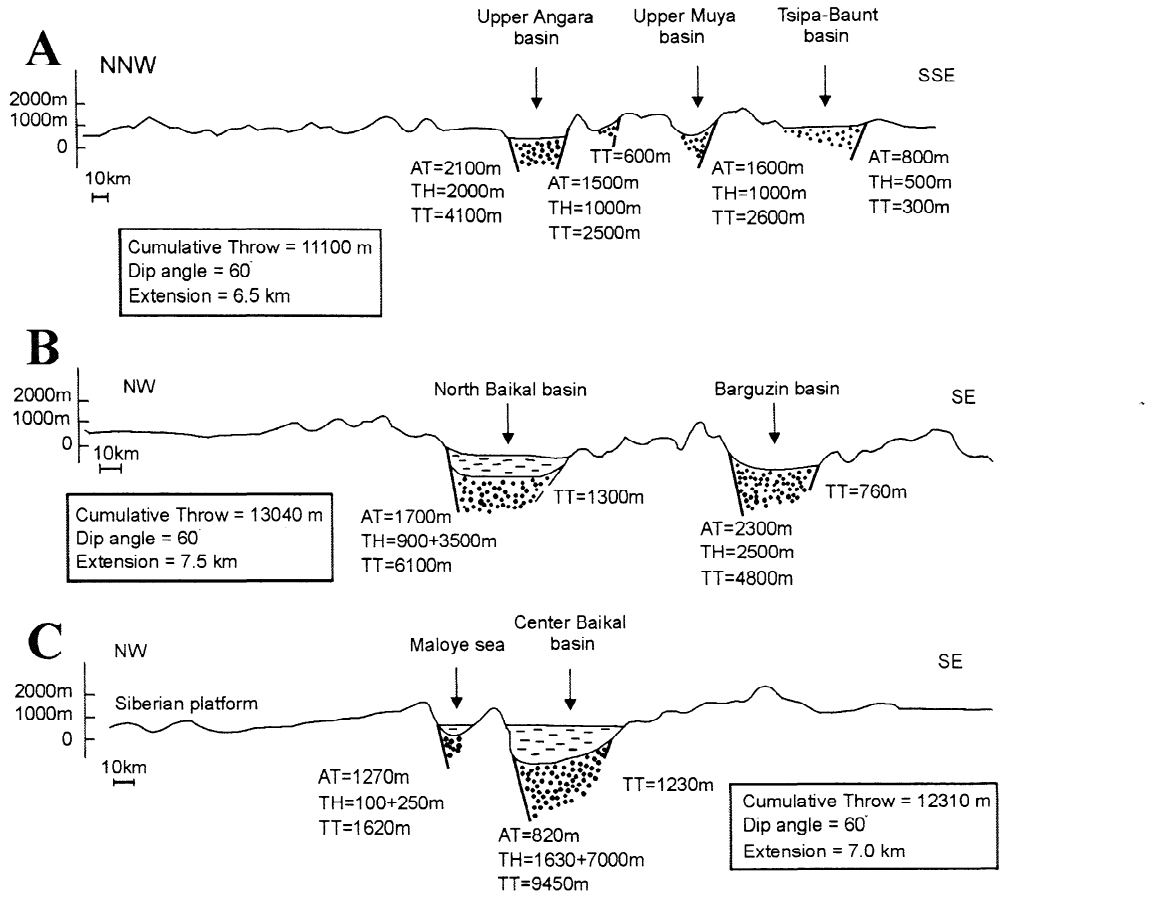

Figure 9. Simplified cross sections perpendicular to strike of border faults in the Baikal Rift, from the northern rift to the central Lake Baikal (location in Figure 8). AT, TH, and TT refer to apparent throw, sediment thickness, and total throw, respectively, estimated for each major and secondary fault on sections, after *Logatchev and Zorin* [1992] and results from this study. Fault dip angle is approximated to 60°. "Extension" is the amount of finite extension deduced from cumulative throws on each section.

and Barguzin basins seem to accommodate together a total amount of extension which is comparable to the one of central Lake Baikal: This implies that they have probably similar ages but lower single extension rates compared to the central Lake Baikal. These similarities also indicate that we should expect rather constant velocity rates across the Baikal Rift from SW to NE, which is indeed what we found by comparing GPS (SW rift) and field study (NE rift) results.

6. Discussion and Conclusions

This study first aims to bring new constraints on fault rates and geometry on individual faults in a part poorly known of the Baikal Rift. In our study region, faults are clearly expressed but are segmented and distributed in a general en échelon pattern: This is the reason why we have included nine new field descriptions and 22 available observations previously made in the region in order to get a quantification of displacements across the rift. We believe that the consistency in vertical shifts, the similar left-lateral component found in scarps trending ~N60°E, and the homogeneity and extent of previously published datings [*Levi et al.*, 1998; *Klein*, 1971; *Grosswald*, 1980; *Back and Strecker*, 1998] are strong reasons for extrapolating the ages found in the Muya region thanks to our new set of 47 ^{14}C samples.

6.1. Segmentation, Inheritance, and Oblique Rifting

Satellite and field observations show that Quaternary and active normal faulting is prominent all over the NBR. The near absence of morphological development of Quaternary strike-slip faulting within this region agrees well with the style of faulting depicted by fault plane solutions of earthquakes, which are dominantly dip slip (see Figure 1) [*Déverchère et al.*, 1993; *Petit et al.*, 1996]. This might suggest that strike-slip faulting is less developed than was estimated by previous authors [*Balla et al.*, 1991; *Doser*, 1991; *Doser and Yarwood*, 1991]. It must be remembered, however, that (1) the en échelon pattern of faults in the limited ~E-W trending deformation zone attests for a significant sinistral component of movement; (2) although weak, left-lateral offsets are often reported on the field; and (3) deposition in basins created by the dip-slip component of faults can hide evidences for strike-slip movement along these faults [*Gaudemer et al.*, 1995]. The reason why en échelon normal faults generally develop instead of strike slip in this region is not

obvious. In our sense, an answer may be found in the structural pattern of the NBR presented above which highlights the relationships of the varying geometry of faults to the preexisting structures. Indeed, two main regions in the NBR may be distinguished:

1. Lake Baikal, along the edge of the Siberian Craton, depicts extensional structures roughly orthogonal to the regional direction of extension and follows the Paleozoic suture zone striking ~N20°E (Figure 8) [*Zamarayev and Ruzhich*, 1978; *Logatchev*, 1993]. There, faults are localized and have large lengths (120-180 km) and high throws, suggesting that they are older and/or display faster rates of extension than faults of the northern rift do. The fact that the suture zone, which limits an old orogenic belt, trends parallel to the deepest depression of the rift (Lake Baikal), provides evidence for the strong influence of the inherited lithospheric fabric on rift initiation and propagation, as observed in many other rifts [e.g., *Vauchez et al.*, 1997 ; *Manighetti et al.*, 1997].

2. Conversely, the ~E-W trending part of the NBR is strongly oblique to the direction of extension but develops inside the Sayan-Baikal belt (Figure 8), which is characterized by a diffuse N60°E structural fabric and a thick crust. Consequently, dip-slip faulting predominates there along these inherited "weak" zones which appear more diffuse than and shorter than zones along the lake (from 10 to 80 km, Figure 7), while the strike-slip component of movement is mostly expressed in the en échelon pattern of faults, and only seldom in the morphology of the young faceted spurs or the seismic activity, as noted above (Figure 1) [*Petit et al.*, 1996].

Moreover, the regular spacing of the half grabens may indicate that their formation has not been triggered by ancient ~N60°E structures but only driven by them. The seismogenic thickness of the lithosphere displays the same size (~30 km) as the mean transverse fault spacing in this region [*Déverchère et al.*, 1993; *Houdry*, 1994], suggesting that this geometry is controlled by the rheological properties of the lithosphere and scale laws [*Jackson and White*, 1989].

Our geometrical observations in the NBR can be compared to experimental modelings of oblique or pull-apart rifting [e.g., *Tron and Brun*, 1991; *Rahe et al.*, 1998; *Basile and Brun*, 1999]. A striking similarity appears between asymmetrical pull-apart models of *Rahe et al.* [1998] and the diamond-shaped Upper Angara basin. Nevertheless, none of the tips of the basins of the NBR turn to strike-slip types, at least during late Quaternary. Although a previous phase of deformation may have been of left-lateral strike-slip type in the Baikal Rift [e.g., *Balla et al.*, 1991; *San'kov et al.*, 1997], we do not detect any clear imprint of that phase on the field. Conversely, at a larger scale a fault pattern very close to the one described in the central (~W-E) deforming zone of the NBR is obtained for a model using a value α (angle between the velocity discontinuity, i.e. the trend of the deforming zone, and the displacement vector) of ~30°-40°, in a rather early stage of oblique rifting [*Tron and Brun*, 1991, Figures 7a and 7b]. Indeed, we found striking similarities between their experiments and our study: (1) Faults are not orthogonal to the extension direction; (2) faults display a typical en échelon distribution with closely spaced overstepping segments; (3) faults depict mostly dip-slip or oblique faulting (with a left-lateral strike-slip component), whereas very rare strike-slip faulting appears only close to the velocity discontinuity (like for the 1957 Muysk earthquake), which indicates slip partitioning (like in the Muya basin); (4) faults delimit long, narrow, and overlapping half grabens; (5) backward (here, counterclockwise) rotation of internal blocks probably occurs (Figure 7) [*Petit et al.*, 1996]; and (6) the predicted angle between the fault trend and the extension vector is ~70° [*Tron and Brun*, 1991, Figure 6] (in the NBR, faults trend around N60°E, and displacement direction is about N130°E). The only significant difference between the experimental model and our observations is the fault length, which seems smaller on the field. This may be explained by several factors, for example, a scaling problem, a more or less favorable network of suitably oriented faults reactivated during rifting, the influence of velocity on viscous coupling in the lower crust, the narrowness of the velocity discontinuity in the experiments [*Tron and Brun*, 1991], or fault shear strength distribution between en échelon segments [*Willemse*, 1997]. Although we cannot discard a possible pull-apart evolution along NE strike-slip faults during the first period of rifting (from ~10 to ~5 Ma [e.g., *San'kov et al.*, 1997 ; *Delvaux et al.*, 1997]), we emphasize our interpretation of oblique rifting (obliquity of ~30°-40°) in the NBR, at least during the fast rifting stage.

6.2. Rift Evolution, Direction, and Rate of Opening

The similar dimensions of several faulted frontal ranges (for generations S1 and S2) and adjacent basins from 110°E to 119°E, together with an examination of the age of basins (Figure 8), suggest that normal faulting started within a short time span in different parts of the NBR, and later than in the south and central Lake Baikal. Hence the idea of a propagating rift from SW to NE is only valid at a very broad scale. Our tentative scheme of rift formation and evolution in the NBR rather favors a progressive development of several half and symmetric grabens in a whole deforming zone that tends to widen with time and to activate new faults of opposite vergence (see the case of Upper Angara), in a way very similar to that shown by experimental modeling of oblique rifting [*Tron and Brun*, 1991, Figure 7]. Additional evidence for oblique rifting is the comparable strike of the mean Holocene displacement vector deduced from our study (~N130°E) and of the stretching vector predicted in the best fit experimental model relative to the boundaries of the deforming zone (~30°-40°) from *Tron and Brun* [1991]. Nevertheless, slip vectors derived from focal mechanisms of earthquakes sometimes indicate less obliquity than Holocene vectors do. We have interpreted these local discrepancies as effects of partitioning between rotating blocks and limits in the spatial extent of fault scarp and focal mechanism samplings. Indeed, the stress directions deduced from both studies (about NW-SE) differ by 25° but remain within uncertainties. A finite element modeling of the Baikal Rift opening [*Lesne et al.*, 1998] provides a best fit model that agrees both in predicted strain and stress directions with our study in the NBR, and with the model of a pole of rotation of Siberian and Amurian plates at the easternmost tip of the Baikal Rift [*Zonenshain and Savostin*, 1981].

Rate of opening deduced from this study is based on levelings of fault scarps on the field and on a new set of ^{14}C datings of postglacial terraces. The lower bound of total horizontal velocity found in this study (~3 mm yr^{-1}) is about 2 times greater than previous hypotheses for the Baikal Rift [e.g., *Zonenshain and Savostin*, 1981] or than predictions of most deformation models

of Asia [e.g., *Holt et al.*, 1995; *Peltzer and Saucier*, 1996; *England and Molnar*, 1997], but our lower bound is quite similar to the GPS-derived extension rate found in the South Baikal Rift [*Calais et al.*, 1998]. Both results point out the relative inadequacy of present global models to describe regional strain rates in the Baikal Rift. This could argue for the effect of other dynamic contributions to intracontinental deformation in north Asia, like a mantle plume [e.g., *Zorin*, 1981; *Gao et al.*, 1994], or the Pacific-Eurasia subduction, in addition to the effect of the Indo-Eurasian collision [*Kong and Bird*, 1996; *Calais et al.*, 1998]. Future GPS campaigns are needed to check the consistency of our field results to instantaneous relative motions of blocks in the NBR and to identify with more details these additional stress contributions. Furthermore, extrapolating our Holocene rates to the timescale of rifting has led us to reasonable estimates of basin ages (although younger than generally believed, i.e., less than 7 Ma) and to a spatial and temporal evolution of rifted basins quite consistent with models of oblique rifting. It suggests that ages of several basins east of 110°E (mainly, Upper Angara, Muya, and Tsipa-Baunt) have been overestimated, whereas throw rates along the northern Lake Baikal and Barguzin basins may have increased with time. Finally, we have found rather constant total vertical throws and amounts of extension (~12 and ~7 km, respectively) across major faults from the central to the northern rift, suggesting a rather homogeneous displacement field over the whole rift in space and time.

Acknowledgments. This study has been carried out in cooperation between the Russian Academy of Science (RAS), University Pierre et Marie Curie, and the French Centre National de la Recherche Scientifique (CNRS). We thank N.A. Logatchev for help in organizing this cooperation. We have benefited from discussions with Eric Calais, Kirill Levi, and Carole Petit, and we have received support from INSU-CNRS programs "Tectoscope-Positionnement" (1992 and 1993) and "Intérieur de la Terre" (1997-1998), Russian Academy of Science, and French Embassy ("Echanges scientifiques") to perform and achieve this work. Many thanks are due to the anonymous reviewers for their helpful revision of the first version of this manuscript. This is Géosciences Azur (CNRS/UPMC/UNSA/IRD) contribution 308.

References

Agar, S.M., and K.D. Klitgord, Rift flank segmentation, basin initiation and propagation: A neotectonic example from Lake Baikal, *J. Geol. Soc. London, 152*, 849-860, 1995.

Angelier, J., and P. Mechler, Sur une méthode graphique de recherche des contraintes principales également utilisable en tectonique et en sismologie: La méthode des dièdres droits, *Bull. Soc. Geol. Fr., XIX*, 651-652, 1977.

Artyushkov, E.V., F.A. Letnikov, and V.V. Ruzhich, The mechanism of formation of the Baikal Rift basin, *J. Geodyn., 11*, 277-291, 1990.

Avouac, J.P., and P. Tapponnier, Kinematic model of deformation in central Asia, *Geophys. Res. Lett., 20*, 895-898, 1993.

Back, S., and M.R. Strecker, Asymmetric late Pleistocene glaciations in the North Baikal basin, Russia, *J. Geol. Soc. London, 155*, 61-70, 1998.

Back, S., M. De Batist, M.R. Strecker, and P. Vanhauwaert, Quaternary depositional systems in northern Lake Baikal, Siberia, *J. Geol., 107*, 1-12, 1999.

Baljinnyam, I., et al., Ruptures of Major Earthquakes and Active Deformation in Mongolia and Its Surroundings, *Mem. Geol. Soc. Am., 181*, 62 pp., 1993.

Balla, Z., M. Kuzmin, and K.G. Levi, Kinematics of the Baikal opening: Results of modeling, *Ann. Tecton., 5*, 18-31, 1991.

Bard, E., B. Hamelin, R.G. Fairbanks, and A. Zindler, Calibration of the ^{14}C timescale over the last 30,000 years using mass spectrometric U-Th ages from Barbados corals, *Nature, 345*, 405-410, 1991.

Basile, C., and J.P. Brun, Transtensional faulting patterns ranging from pull-apart basins to transform continental margins: An experimental investigation, *J. Struct. Geol., 21*, 23-38, 1999.

Bazarov, D.B., I.N. Rezanov, and R.C. Budaev, *Geomorphology of North Pribaikalye and Stanovoy Ridge* (in Russian), 198 pp., Nauka, Moscow, 1981.

Calais, E., O. Lesne, J. Déverchère, V. San'kov, A. Lukhnev, A. Miroshnitchenko, V. Buddo, K. Levi, V. Zalutzky, and Y. Baskhuev, Crustal deformation in the Baikal Rift from GPS measurements, *Geophys. Res. Lett.*, 25, 4003-4006, 1998.

Colman, S.M., J.A. Peck, E.B. Karabanov, S.J. Carter, J.P. Bradbury, J.W. King, and D.F. Williams, Continental climate response to orbital forcing from biogenic silica records in Lake Baikal, *Nature, 378*, 769-771, 1995.

Delvaux, D., R. Moeys, G. Stapel, C. Petit, K.G. Levi, A. Miroshnichenko, V.V. Ruzhich, and V.A. San'kov, Paleostress reconstruction and geodynamics of the Baikal region, central Asia, II, Cenozoic rifting, *Tectonophysics, 282*, 1-38, 1997.

Déverchère, J., F. Houdry, M. Diament, N.V. Solonenko, and A.V. Solonenko, Evidence for a seismogenic upper mantle and lower crust in the Baikal Rift, *Geophys. Res. Lett., 18*, 1099-1102, 1991.

Déverchère, J., F. Houdry, N.V. Solonenko, A.V. Solonenko, and V.A. Sankov, Seismicity, active faults and stress field of the North Muya region, Baikal Rift: New insights on the rheology of extended continental lithosphere, *J. Geophys. Res., 98*, 19,895-19,912, 1993.

Doser, D.I., Faulting within the eastern Baikal Rift as characterized by earthquake studies, *Tectonophysics, 196*, 109-139, 1991.

Doser, D.I., and D.R. Yarwood, Strike-slip faulting in continental rifts: Examples from Sabukia, East Africa (1928) and other regions, *Tectonophysics, 197*, 213-224, 1991.

Endrikhinsky, A.S., S.S. Osadchiy, and S.V. Rasskazov, *Geology and Seismicity of the Baikal-Amur Railroad Zone: Cenozoic deposits and geomorphology* (in Russian), Nauka, Moscow, 170 pp., 1983.

England, P., and P. Molnar, The field of crustal velocity in Asia calculated from Quaternary rates of slip faults, *Geophys. J. Int., 130*, 551-582, 1997.

Gao, S., P.M. Davis, H. Liu, P.D. Slack, Y.A. Zorin, N.A. Logatchev, M.G. Kogan, P.D. Burkholder, and R.P. Meyer, Asymmetric upwarp of the asthenosphere beneath the Baikal Rift zone, Siberia, *J. Geophys. Res., 99*, 15,319-15,330, 1994.

Gasse, F., et al., A 13,000 yr climatic record in western Tibet, *Nature, 353*, 742-745, 1991.

Gaudemer, Y., P. Tapponnier, and D.L. Turcotte, River offsets across active strike-slip faults, *Ann. Tecton., 3*, 55-76, 1989.

Gaudemer, Y., P. Tapponnier, B. Meyer, G. Peltzer, G. Shunmin, C. Zhitai, D. Huagung, and I. Cifuentes, Partitioning of crustal slip between linked, active faults in the eastern Qilian Shan, and evidence for a major seismic gap, the "Tianzhu gap", on the western Haiyuan fault, Gansu, China, *Geophys. J. Int., 120*, 599-645, 1995.

Golenetsky, S.I., Problems of the seismicity of the Baikal Rift zone, *J. Geodyn., 11*, 293-307, 1990.

Grosswald, M.G., Late Weichselian ice sheet of northern Eurasia, *Quat. Res., 13*, 1-32, 1980.

Holt, W.E., M. Li, and A.J. Haines, Earthquake strain rates and instantaneous relative motions within central and eastern Asia, *Geophys. J. Int., 122*, 569-593, 1995.

Houdry, F., Mécanismes de l'extension continentale dans le rift Nord-Baïkal, Sibérie: Contraintes des données d'imagerie SPOT, de terrain, de sismologie et de gravimétrie, thèse de doctorat, 345 pp., Univ. Pierre et Marie Curie (Paris VI), Paris, 1994.

Hutchinson, D.R., A.J. Golmshtok, L.P. Zonenshain, T.C. Moore, C.A. Scholz, and K.D. Klitgord, Depositional and tectonic framework of the rift basins of Lake Baikal from multichannel seismic data, *Geology, 20*, 589-592, 1992.

Jackson, J., and N. White, Normal faulting in the upper continental crust: Observations from areas of active extension, *J. Struct. Geol., 11*, 15-36, 1989.

Klein, R., The Pleistocene prehistory of Siberia, *Quat. Res., 1*, 133-161, 1971.

Kong, X., and P. Bird, Neotectonics of Asia: Thin-shell finite-element models with faults, in *The Tectonic Evolution of Asia*, edited by A. Yin and T.M. Harrison, pp. 19-34, Cambridge Univ. Press, New York, 1996.

Kulchitsky A.A., T.M. Skovitina, and G.F. Ufimzev, *Damp Lakes in the Rifts of East Siberia: Evidences from the Past and Probability in the Future* (in Russian), Geogr. and Nat. Res., pp. 61-65, Irkutsk, 1997.

Lesne, O., E. Calais, and J. Déverchère, Finite element modelling of crustal deformation in the Baikal Rift zone: New insights into the active-passive debate, *Tectonophysics, 289*, 327-430, 1998.

Levi, K.G., et al., Postglacial tectonics in the Baikal Rift (in Russian), *Russ. J. Earth Sci.*, 1,

pap. 1, 1998. (Available at http://eos.wdcb.rssi.ru/tjes/tjes_e00.htm).

Logatchev, N.A., History and geodynamics of the Lake Baikal Rift in the context of the eastern Siberia rift system: A review, *Bull. Cent. Rech. Explor. Prod. Elf Aquitaine, 17*, 353-370, 1993.

Logatchev, N.A., and Y.A. Zorin, Evidence and causes of the two-stage development of the Baikal Rift, *Tectonophysics, 143*, 225-234, 1987.

Logatchev, N.A., and Y.A. Zorin, Baikal Rift Zone: Structure and geodynamics, *Tectonophysics, 208*, 273-286, 1992.

Manighetti, I., P. Tapponnier, V. Courtillot, S. Gruszow, and P.Y. Gillot, Propagation of rifting along the Arabia-Somalia plate boundary: The Gulfs of Aden and Tadjoura, *J. Geophys. Res., 102*, 2681-2710, 1997.

Mats, V.D., The structure and evolution of the Baikal Rift depression, *Earth Sci. Rev.*, 34, 81-118, 1993.

Peck, J.A., J.W. King, S.M. Colman, and V.A. Kravchinsky, A rock-magnetic record from Lake Baikal, Siberia: Evidence for late Quaternary climate change, *Earth Planet. Sci. Lett., 122*, 221-238, 1994.

Peltzer, G., and F. Saucier, Present-day kinematics of Asia derived from geologic fault rates, *J. Geophys. Res., 101*, 27,943-27,956, 1996.

Peltzer, G., P. Tapponnier, Y. Gaudemer, B. Meyer, G. Shunmin, Y. Kelun, C. Zhitai, and D. Huagung, Offsets of late Quaternary morphology, rate of slip, and recurrence of large earthquakes on the Chang Ma fault (Gansu, China), *J. Geophys. Res., 93*, 7793-7812, 1988.

Petit, C., J. Déverchère, F. Houdry, V.A. Sankov, V.I. Melnikova, and D. Delvaux, Present-day stress field changes along the Baikal Rift and tectonic implications, *Tectonics, 15*, 1171-1191, 1996.

Rahe, B., D.A. Ferril, and A.P. Morris, Physical analog modeling of pull-apart basin evolution, *Tectonophysics, 285*, 21-40, 1998.

Ritz, J.F., E.T. Brown, D. Bourlès, H. Philip, A. Schlupp, G. Raisbeck, F. Yiou, and E. Enhtuvshin, Slip rates along active faults estimated with cosmic ray exposure dates: Application to the Bogd fault, Gobi-Altai, Mongolia, *Geology, 23*, 1019-1022, 1995.

San'kov, V.A., A.I. Miroshnichenko, K.G. Levi, A.V. Lukhnev, A.I. Melnikov, and D. Delvaux, Cenozoic stress field evolution in the Baikal Rift zone, *Bull. Cent. Rech. Explor. Prod. Elf Aquitaine, 21*, 435-455, 1997.

Solonenko, A.V., N.V. Solonenko, V.I. Melnikova, B.M. Kuzmin, O.A. Kuchai, and S.S. Sukhanova, Stresses and fault plane motions of earthquakes in Siberia and Mongolia, in *Seismicity and Seismic Zoning of Northern Eurasia* (in Russian), vol. 1, pp. 113-122, Institute of Physics of the Earth, Moscow, 1993.

Solonenko, A.V., N.V. Solonenko, V.I. Melnikova, and E. Shteiman, The seismicity and earthquake focal mechanisms of the Baikal Rift zone, *Bull. Cent. Rech. Explor. Prod. Elf Aquitaine, 21*, 207-231, 1997.

Solonenko, V.P., *Seismic Regional Division of Eastern Siberia and its Geological and Geophysical Base* (in Russian), 162 pp., Nauka, Moscow, 1977.

Solonenko, V.P., V.V. Nikolaev, R.M. Semyonov, M.G. Demyanovitch, R.A. Kurushin, V.S. Khromovskikh, and A.V. Tchipizubov, Geology and Seismicity of the BAM (Baikal-Amur Main) Railway Zone (in Russian), vol. 8, 189 pp., Nauka, Moscow, 1985.

Tapponnier, P., and P. Molnar, Active faulting and cenozoic tectonics of the Tien Shan, Mongolia and Baykal regions, *J. Geophys. Res., 84*, 3425-3459, 1979.

Trofimov, A.G., Space-time changes of fluvial processes in North Pribaikalye, in *Time and Age of the Relief* (in Russian), edited by N.A. Logatchev, D.A. Timofeev, and G.F. Ufimzev, pp. 119-124, Nauka, Moscow, 1994.

Tron, V., and J.P. Brun, Experiments on oblique rifting in brittle-ductile systems, *Tectonophysics, 188*, 71-84, 1991.

Van der Beek, P., Flank uplift and topography at the central Baikal Rift (SE Siberia): A test of kinematic models for continental extension, *Tectonics, 16*, 122-136, 1997.

Van der Beek, P.A., D. Delvaux, P.A.M. Andriessen, and K.G. Levi, Early Cretaceous denudation related to convergent tectonics in the Baikal region, SE Siberia, *J. Geol. Soc. London, 153*, 515-523, 1996.

Van der Woerd, J., F.J. Ryerson, P. Tapponnier, Y. Gaudemer, R. Finkel, A.S. Mériaux, M. Caffee, G. Zhao, and Q. He, Holocene left-slip rate determined by cosmogenic surface dating on the Xidatan segment of the Kunlun fault (Qinghai, China), *Geology, 26*, 695-698, 1998.

Vauchez, A., G. Barruol, and A. Tommasi, Why do continents break-up parallel to ancient orogenic belts?, *Terra Nova, 9*, 62-66, 1997.

Wallace, R.E., Profiles and ages of young fault scarps, north-central Nevada, *Geol. Soc. Am. Bull., 88*, 1267-1281, 1977.

Willemse, E.J.M., Segmented normal faults: Correspondence between three-dimensional mechanical models and field data, *J. Geophys. Res., 102*, 675-692, 1997.

Zamarayev, S.M., and V.V. Ruzhich, On relationships between the Baikal Rift and ancient structures, *Tectonophysics, 45*, 41-47, 1978.

Zhang, Y.Q., J.L. Mercier, and P. Vergély, Extension in the graben systems around the Ordos (China), and its contribution to the extrusion tectonics of South China with respect to Gobi-Mongolia, *Tectonophysics, 285*, 41-75, 1998.

Zonenshain, L.P., and L.A. Savostin, Geodynamics of the Baikal Rift zone and plate tectonics of Asia, *Tectonophysics, 76*, 1-45, 1981.

Zorin, Y.A., The Baikal Rift: An example of the intrusion of asthenospheric material into the lithosphere as the cause of disruption of the lithosphere plates, *Tectonophysics, 73*, 91-104, 1981.

Zorin, Y.A., and L. Cordell, Crustal extension in the Baikal Rift zone, *Tectonophysics, 198*, 117-121, 1991.

J. Déverchère and F. Houdry, Géosciences Azur, UMR 6526, Observatoire Océanologique, Université Pierre et Marie Curie, BP48, F-06235 Villefranche sur Mer, France. (jack@obs-vlfr.fr)

A. Filippov and V. San'kov, Institute of the Earth's Crust, Siberian Branch, Russian Academy of Science, Lermontov street 128, 664033 Irkutsk, Russia.

Y. Gaudemer, Laboratoire de Tectonique, UMR 7578, Institut de Physique du Globe, 4 Place Jussieu, F-75252 Paris, France.

(Received June 21, 1999;
revised January 14, 2000;
accepted February 21, 2000.)